

See discussions, stats, and author profiles for this publication at: <https://www.researchgate.net/publication/266263799>

Hydrogen/Deuterium Exchange–Protected Oligomers Populated during A β Fibril Formation Correlate with Neuronal Cell Death

ARTICLE in ACS CHEMICAL BIOLOGY · SEPTEMBER 2014

Impact Factor: 5.33 · DOI: 10.1021/cb500621x · Source: PubMed

CITATIONS

4

READS

41

6 AUTHORS, INCLUDING:



Bernat Serra-Vidal
Centre for Genomic Regulation
2 PUBLICATIONS 16 CITATIONS

[SEE PROFILE](#)



Sergio Madurga
University of Barcelona
40 PUBLICATIONS 472 CITATIONS

[SEE PROFILE](#)

Hydrogen/Deuterium Exchange-Protected Oligomers Populated during A β Fibril Formation Correlate with Neuronal Cell Death

Bernat Serra-Vidal,[†] Lluís Pujadas,[‡] Daniela Rossi,[‡] Eduardo Soriano,^{‡,§} Sergio Madurga,^{||} and Natàlia Carulla*,[†]

[†]Institute for Research in Biomedicine (IRB Barcelona), Baldiri Reixac 10, Barcelona 08028, Spain

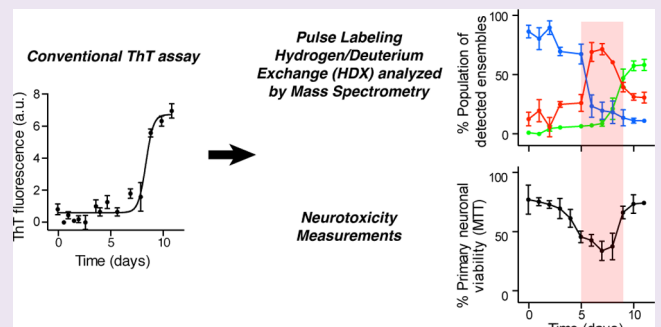
[‡]Department of Cell Biology, University of Barcelona and Centro de Investigación en Red sobre Enfermedades Neurodegenerativas (CIBERNED), Diagonal 647, Barcelona 08028, Spain

[§]CIEN Foundation, Madrid 28031, Spain

^{||}Department of Physical Chemistry and Research Institute of Theoretical and Computational Chemistry (IQT-CUB), University of Barcelona, Martí i Franquès 1, Barcelona 08028, Spain

Supporting Information

ABSTRACT: The aggregation of the amyloid- β peptide (A β) to form fibrils and plaques is strongly associated with Alzheimer's disease (AD). Although it is well established that this process generates neurotoxicity, it is also heterogeneous with a variety of species being formed during the conversion process. This heterogeneity makes it difficult to detect and characterize each of the aggregates formed, which precludes establishing the specific features responsible for the neurotoxicity observed. Here we use pulse-labeling hydrogen-deuterium exchange experiments analyzed by electrospray ionization mass spectrometry (PL-HDX-ESI-MS) to distinguish three ensembles populated during the aggregation of the 40 and 42 residue forms of the A β peptide, A β 40 and A β 42, on the basis of differences in their persistent structure. Noticeably, two of them are more abundant at the beginning and at the end of the lag phase and are therefore not detectable by conventional assays such as Thioflavin T (ThT). The ensembles populated at different stages of the aggregation process have a surprisingly consistent average degree of exchange, indicating that there are definite structural transitions between the different stages of aggregation. To determine whether an ensemble of species with a given hydrogen exchange pattern correlates with neurotoxicity, we combined PL-HDX-ESI-MS experiments with parallel measurements of the neurotoxicity of the samples under study. The results of this dual approach show that the maximum toxicity correlates with the ensemble comprising HDX protected oligomers, indicating that development of persistent structure within A β oligomers is a determinant of neurotoxicity.



The origin and progression of Alzheimer's disease (AD) has been linked to the aggregation of A β .¹ A β aggregation, a highly heterogeneous process, involves the sequential formation of a variety of soluble oligomeric assemblies that ultimately evolve into long and unbranched amyloid fibrils that possess a highly characteristic cross- β sheet structure where the strands are oriented perpendicular to the fibril long axis.² Amyloid fibrils are the major components of the extracellular plaques found in the brains of AD patients. The abundance of fibrillar amyloid plaques in brain tissue is, however, only weakly associated with the severity of dementia.³ Indeed, there appears to be a stronger correlation between the levels of A β oligomers in the brain and the degree of cognitive deficit,⁴ such that oligomers are now widely considered to be the pathogenic molecular forms of A β in AD and consequently have been singled out as drug targets to address this disease.⁵

Despite their implication as the major agents in AD, A β oligomers are a challenging therapeutic target as they are much

more dynamic and heterogeneous than amyloid fibrils, the end products of A β aggregation.⁶ To overcome their dynamic nature, considerable efforts have been directed to obtain stable A β oligomer preparations.^{7–11} However, various reports point to the importance of studying simultaneously all of the species populated during A β aggregation. These include the findings that catalytic amounts of fibrillar aggregates catalyze the conversion of monomers into neurotoxic oligomers through secondary nucleation¹² and that the process of aggregation, rather than discrete oligomer species, is responsible for inducing neurotoxicity.^{13,14} To characterize simultaneously all of the species that form during aggregation, the heterogeneous nature of the process needs to be overcome. In this context, important methodological advances have been made, including

Received: August 5, 2014

Accepted: September 15, 2014

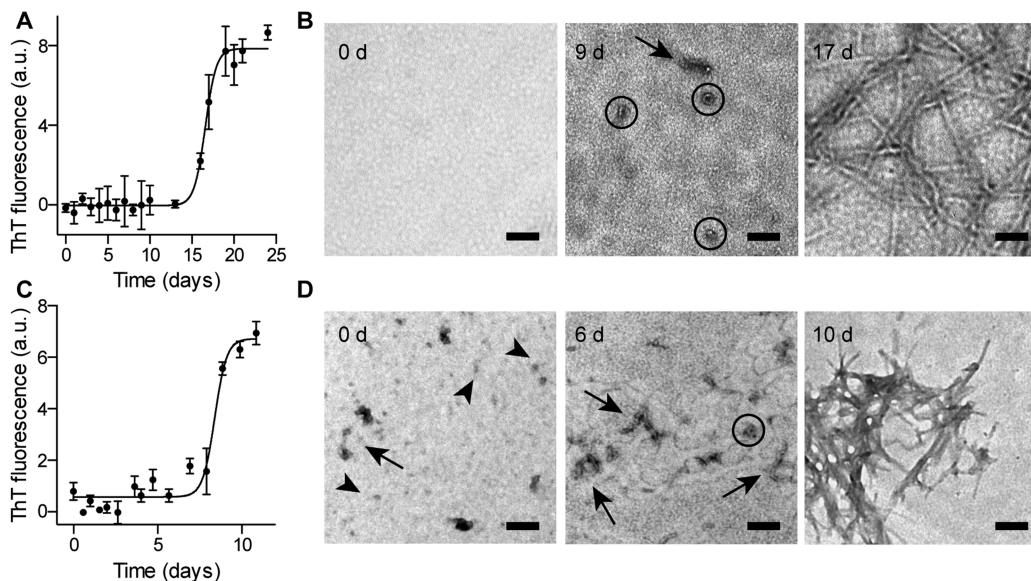


Figure 1. Characterization of $\text{A}\beta$ 40 and $\text{A}\beta$ 42 aggregation under ESI-MS-compatible buffer conditions. Thirty micromolar $\text{A}\beta$ samples were left incubating at 25 °C in 50 mM NH_4OAc , 1 mM Tris, and 0.01% NaN_3 at pH 7.4. ThT binding measurements obtained at a range of aggregation times for (A) $\text{A}\beta$ 40 and (C) $\text{A}\beta$ 42. Electron micrographs obtained for (B) 0, 9, and 17 days of $\text{A}\beta$ 40 and (D) 0, 6, and 10 days of $\text{A}\beta$ 42 aggregation. Annular assemblies of about 25–35 nm diameter are shown as circles, short curvilinear filaments of up to 100 nm in length, referred to as protofibrils in the literature, as arrows, and compact spherical particles roughly 4–5 nm in diameter as arrowheads. Scale bar represents 100 nm.

the use of ion mobility mass spectrometry¹⁵ and single molecule fluorescence techniques.¹⁶ However, due to the nature of these techniques, they are most suitable to study the initial stages of aggregation.

Hydrogen-deuterium exchange experiments (HDX) are based on solvent accessibility. Hydrogen atoms in stable hydrogen bonds exhibit significant protection. In contrast, rapid exchange can take place at amide groups not involved in hydrogen bonds and that are accessible to the solvent.¹⁷ The ~1 Da mass difference between hydrogen and deuterium allows tracking of HDX events as well as detecting distinct populations of molecules with different degree of exchange by electrospray ionization mass spectrometry (ESI-MS). Therefore, provided that different aggregates adopt different structures, HDX-ESI-MS offers a powerful opportunity to detect them. In fact, this strategy has been successfully applied to characterize the structure of stabilized $\text{A}\beta$ oligomers^{18–20} as well as other protein oligomers implicated in related neurodegenerative conditions.^{21,22} Moreover, by using kinetic HDX experiments such as pulse-labeling HDX-ESI-MS (PL-HDX-ESI-MS) together with a fractionation step, the protection of soluble $\text{A}\beta$ 42 oligomers has been recently monitored as a function of time.²³ Using a model amyloidogenic protein, we employed PL-HDX-ESI-MS experiments combined with a strategy in which instead of fractionating, we dissolved all of the aggregates into their constituent monomers, which allowed us to detect and characterize the distinct species present during amyloid fibril formation.²⁴ Extension of this approach to the study of $\text{A}\beta$ aggregation offers a powerful opportunity to probe this process, allowing for the first time the characterization of $\text{A}\beta$ oligomers, together with all other species that form during aggregation.

Here we have used this PL-HDX-ESI-MS strategy to study $\text{A}\beta$ 40 and $\text{A}\beta$ 42 aggregation *in vitro* under physiological conditions and show that in each case three distinct structural ensembles are detected in different relative abundances during the aggregation process. Since the ensembles exhibit a surprisingly consistent average degree of exchange, their

detection indicates that there are definite structural transitions during $\text{A}\beta$ aggregation. Finally, in conjunction with parallel experiments designed to assess primary neuronal viability, the nature of the toxicity could be correlated with the ensembles detected. From analysis of our tandem PL-HDX-ESI-MS and neurotoxicity experiments, we conclude that the ensemble comprising HDX protected oligomers is the most strongly associated with the neurotoxicity observed.

RESULTS AND DISCUSSION

Properties of $\text{A}\beta$ Aggregates, Formed under MS-Compatible Buffer Conditions, Are Preserved. To characterize $\text{A}\beta$ 40 and $\text{A}\beta$ 42 aggregation using PL-HDX-ESI-MS, we chose an aggregation buffer that would be as compatible as possible with MS analysis, in order to avoid the use of long desalting times, and that would also allow the formation of the same types of aggregates as previously reported in the literature.^{5,25} 50 mM NH_4OAc , 1 mM Tris, and 0.01% NaN_3 at pH 7.4 was found to fulfill both requirements. Using size-exclusion chromatography (SEC), $\text{A}\beta$ 40 and $\text{A}\beta$ 42 were eluted in this buffer in their monomeric state and allowed to aggregate at 25 °C without shaking. To examine whether the soluble oligomeric assemblies and fibrils formed under these conditions are the same as those previously reported,^{5,25} we first monitored the aggregation of 30 μM $\text{A}\beta$ 40 and of $\text{A}\beta$ 42 under the conditions described above using the well-established ThT fluorescence assay (Figure 1A and C). This assay relies on the capacity of the ThT dye to bind amyloid fibrils; upon fibril binding, the fluorescence properties of the dye change, thus allowing the monitoring of fibril formation.²⁶ $\text{A}\beta$ 40 and $\text{A}\beta$ 42 fibril formation exhibited the characteristic sigmoidal ThT profile (Figure 1A and C) and involved an initial lag phase of 15 days and 7.5 days, respectively, followed by a growth phase that led to a plateau phase in which complete fibril formation occurred after 19 and 9 days, respectively.

To learn about the morphology of the aggregates formed during aggregation, we analyzed by Transmission Electron

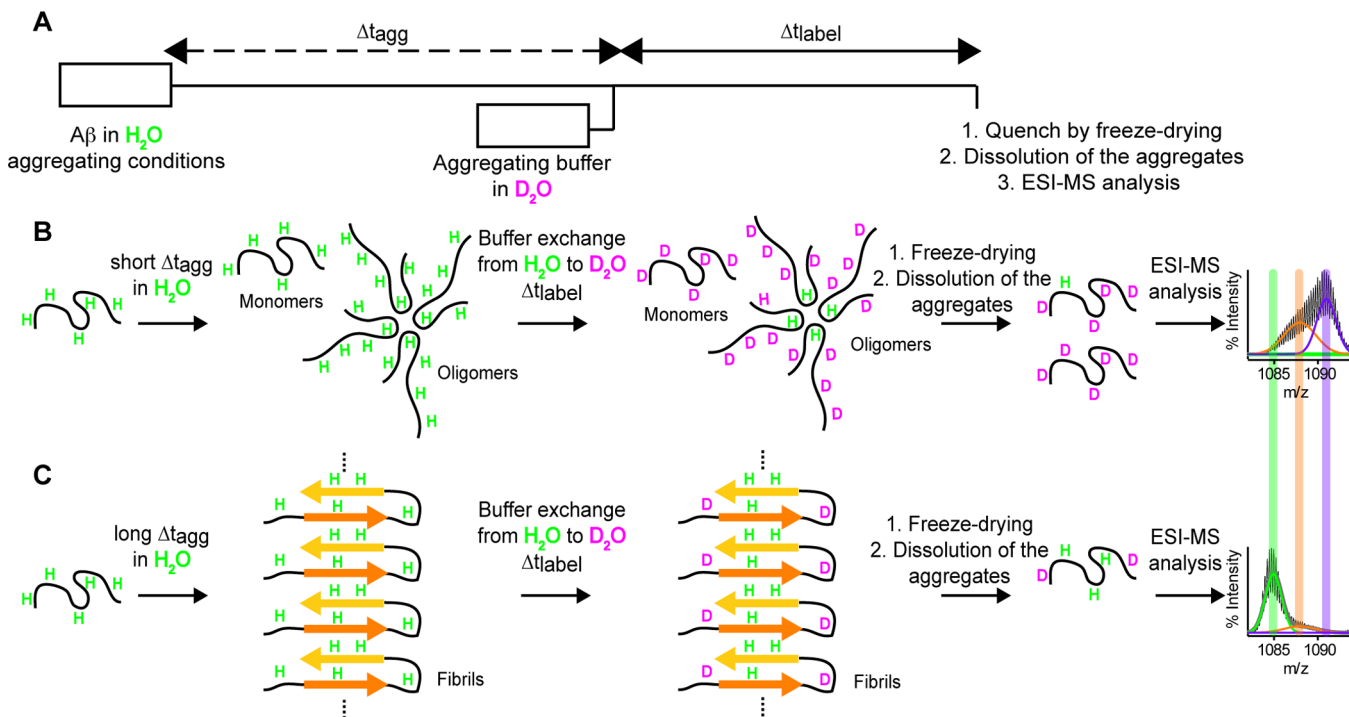


Figure 2. Schematic description of the PL-HDX-ESI-MS experiment used to study $\text{A}\beta 40$ and $\text{A}\beta 42$ aggregation. (A) The experiment starts by incubating soluble $\text{A}\beta$ peptide under aggregation conditions in a protonated buffer. After a variable aggregation time, Δt_{agg} , labeling takes place for a fixed period of time, Δt_{label} , using deuterated aggregation buffer. After the labeling pulse, freeze-drying is used to quench exchange. Different samples are prepared at defined Δt_{agg} , which are later solubilized into monomers by transfer to a DMSO solution and analyzed by ESI-MS. The figure illustrates hypothetical scenarios when the peptide is left to aggregate for (B) a short Δt_{agg} and (C) a long Δt_{agg} .

Microscopy (TEM) aliquots of the aggregating solutions at specific time points (Figure 1B and D). At the beginning of the lag phase of $\text{A}\beta 40$ aggregation, aggregates were rarely seen; toward the end of this phase a mixture of oligomeric assemblies with different morphologies ranging from annular assemblies of about 25–35 nm in diameter (shown as circles in Figure 1B) to short curvilinear filaments of up to 100 nm in length, referred to in the literature as protofibrils, were detected (shown as arrows in Figure 1B). In agreement with the ThT assay, well-defined $\text{A}\beta 40$ fibrils were observed from 13 days onward (Figure 1B). At the beginning of the lag phase of $\text{A}\beta 42$ aggregation, compact spherical particles roughly 4–5 nm in diameter (shown as arrowheads in Figure 1D) together with short curvilinear protofibrils of up to 100 nm in length (shown as arrows in Figure 1D) were observed. The latter became more abundant toward the end of this phase together with the observation of annular assemblies of about 25–35 nm in diameter (shown as circles in Figure 1D). During the plateau phase, in accordance with the ThT fluorescence measurements, $\text{A}\beta 42$ fibrils were the most abundant species observed in the TEM images (Figure 1D).

Finally, the $\text{A}\beta 40$ and $\text{A}\beta 42$ fibrils formed during the plateau phase were characterized using X-ray fiber diffraction (Supplementary Figure S1). We observed the two reflections characteristic of the cross- β sheet structure for these fibrils: a meridional reflection at 4.7 Å and an equatorial reflection at 10.4 Å. These reflections are a fundamental property of all amyloid fibrils characterized to date. Taken together, results from ThT assays, TEM, and X-ray diffraction indicate that under the MS-compatible buffer conditions used here, the intrinsic characteristics of the soluble oligomeric assemblies, including compact spherical particles, annular assemblies as well

as short, curvilinear protofibrils, and the fibrils formed are the same as those previously described,^{5,25} although with slower kinetics of aggregation. Moreover, as thoroughly shown in the literature, under our MS-compatible buffer conditions, $\text{A}\beta 40$ fibril formation is slower than that of $\text{A}\beta 42$ (half time of fibril formation was 16.6 ± 0.1 days and 8.4 ± 0.2 days for $\text{A}\beta 40$ and $\text{A}\beta 42$, respectively).

PL-HDX-ESI-MS Experiments Detect Three Ensembles during $\text{A}\beta$ Fibril Formation. After establishing MS-compatible buffer conditions in which to study $\text{A}\beta 40$ and $\text{A}\beta 42$ aggregation, we probed the species present during this process by means of PL-HDX-ESI-MS experiments (Figure 2). Briefly, the experiments were initiated by incubating the two $\text{A}\beta$ variants under the conditions described in the previous section. Each peptide was left to aggregate over a range of time periods (Δt_{agg}), and after each different value of Δt_{agg} , the solution was diluted in deuterium oxide for a fixed “labeling” time (Δt_{label}). During Δt_{label} , labile hydrogen atoms in solvent-accessible regions of the aggregates underwent isotope exchange to incorporate deuterium atoms, whereas those in protected regions remained unexchanged. After each Δt_{label} , the samples were freeze-dried to quench exchange and to trap into the peptide molecules the isotopes present at the different positions. By using different Δt_{agg} and a fixed Δt_{label} , the most exposed regions of each of the aggregates were labeled.

To analyze deuterium incorporation into the peptide molecules present in the aggregates, the latter species were dissociated into their constituent monomers by transfer to a DMSO solution, which also retains the exchange information,²⁷ passed through a C8 desalting column, and then analyzed by ESI-MS. HDX takes place at labile amide protons in the backbone and labile hydrogens in the side chains (e.g., O—H,

N–H, and S–H). However, since the latter exchange much faster than labile amide protons, this deuterium is lost during the desalting step due to back exchange and thus does not contribute to the measured mass shifts. The replacement of each labile amide proton with a deuterium atom increases the mass of the peptide by 1 Da. Since analysis of the exchanged samples by ESI-MS allows detecting populations of molecules with different degrees of exchange, using the PL-HDX-MS-ESI approach, it is possible to overcome the heterogeneity of the aggregation process.²⁴ For a given Δt_{agg} , the number of peaks detected reveals the number of aggregates with different degrees of HDX and consequently with a distinct structure. Moreover, the width of the peaks at half height indicates whether the peaks result from overlap of multiple species with slight differences in the degree of exchange.

The PL-HDX-ESI-MS analysis of A β 40 and A β 42 samples indicated that aggregation occurred as a multistate process, with species entrapping different numbers of deuterium atoms growing, coexisting, and decaying with time (Figure 3A and B). Since protection between species was not different enough to provide well-resolved peaks, mass spectra obtained at different Δt_{agg} for each A β variant were fitted globally using a multi-Gaussian approach. This approach allowed accurate identification of low populated species in one mass spectrum because their position and width were determined in other mass spectra where these species were most abundant. Global analysis of ESI mass spectra revealed that three distinct species had formed during both A β 40 and A β 42 aggregation (Figure 3A,B and Supplementary Figure S2). A plot of the area of each peak, representing each of the ensembles, as a function of the aggregation time, Δt_{agg} , indicated that some species coexisted for significant periods of time (Figure 4A and B). Moreover, in relation with the conventional ThT binding assay, two of the three species detected were more abundant during the silent lag phase of aggregation, one at the beginning and the other at the end (Figure 4A and B). The relative abundance of the third species detected paralleled the development of ThT fluorescence (Figure 4A and B). Therefore, by using PL-HDX-ESI-MS experiments, we have obtained information on the relative population of two species not detectable by conventional assays.

Next, we determined the structural properties of each of the species detected during A β 40 and A β 42 aggregation based on their HDX behavior. At the beginning of the A β 40 ThT lag phase, from 1 to 8 days (Figures 3A and 4A), the most abundant peak corresponded to the mass of the peptide with very little protection; of the 39 amide protons, 38.4 ± 0.5 had exchanged to deuterons (Figure 3C) and presented a width at half height of 2.3 ± 0.4 (Figure 3E). When lyophilized monomeric A β 40 is dissolved in the same DMSO buffer used to solubilize the aggregates into their constituent monomers, the peak width is 1.3 ± 0.1 (Supplementary Figure S3); we took this value as that corresponding to a single species. Therefore, the HDX properties associated with the most abundant peak at the beginning of A β 40 lag phase indicated that it represented an overlap of multiple species with different but negligible protection, and as such, we denoted it as $[\text{M}/\text{O}]_{\text{UP},\text{A}\beta 40}$ to represent unprotected monomers and/or oligomers of A β 40. In contrast, the most abundant peak detected at the beginning of the A β 42 ThT lag phase, from 1 to 5 days (Figure 3B), corresponded to the mass of the peptide with low but significant protection; of the 41 amides available for exchange in A β 42, we detected an average of 33.1 ± 0.8

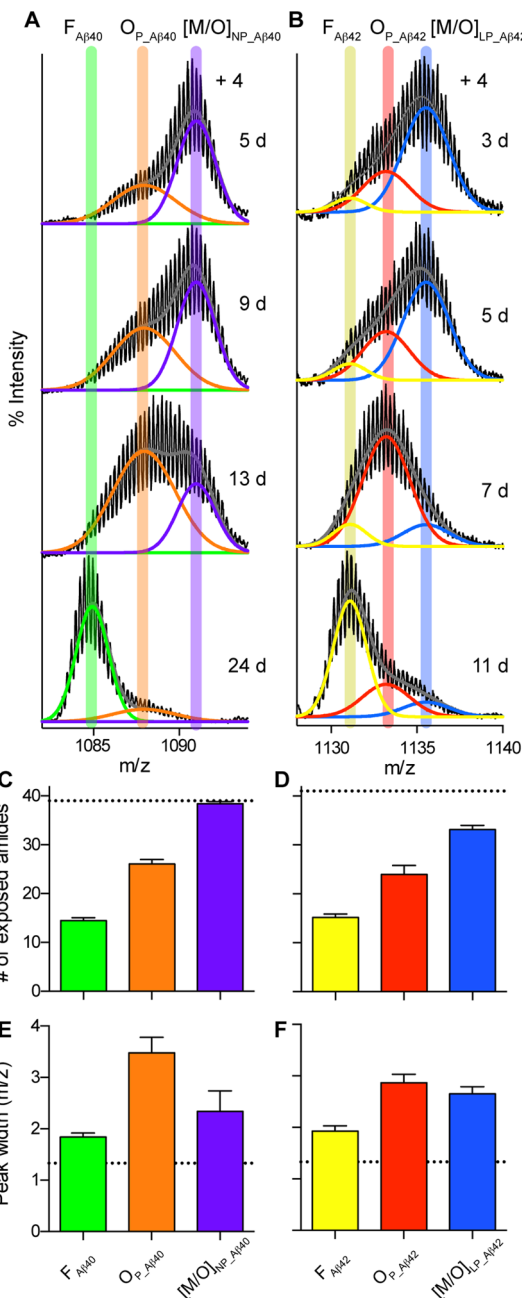


Figure 3. Detection and characterization of distinct ensembles populated during A β 40 and A β 42 aggregation using PL-HDX-ESI-MS. ESI-MS mass spectra (+4 charge state). The spectra show the relative populations of species detected during (A) A β 40 aggregation and (B) A β 42 aggregation at the indicated Δt_{agg} . Peak intensities are normalized to the overall species population. Number of exposed amides for each ensemble during (C) A β 40 aggregation and (D) A β 42 aggregation. Dashed lines in panels C and D correspond, respectively, to the number of available amides for exchange in A β 40 and A β 42. Peak width for each of the detected species during (E) A β 40 aggregation and (F) A β 42 aggregation. Dashed lines in panels E and F correspond to the peak width of the resulting peak obtained from dissolving lyophilized A β 40 in the same DMSO-based buffer used to analyze HDX samples. The ensembles of species detected during A β 40 aggregation are depicted as $[\text{M}/\text{O}]_{\text{NP},\text{A}\beta 40}$ (purple), $O_{\text{P},\text{A}\beta 40}$ (orange), and $F_{\text{A}\beta 40}$ (green) and during A β 42 aggregation as $[\text{M}/\text{O}]_{\text{LP},\text{A}\beta 42}$ (blue), $O_{\text{P},\text{A}\beta 42}$ (red), and $F_{\text{A}\beta 42}$ (yellow). The data are the mean \pm SD of three experiments.

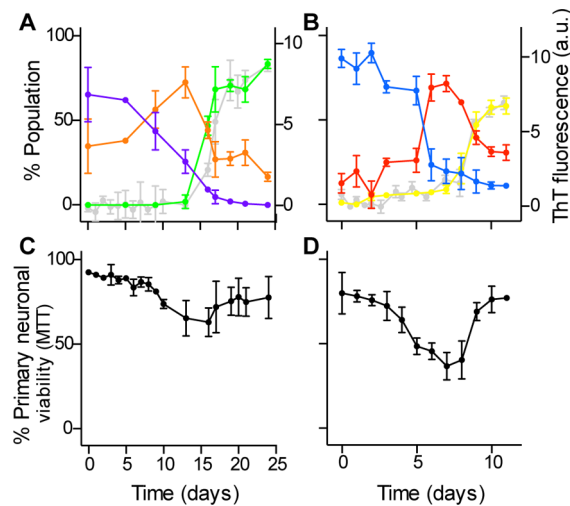


Figure 4. Ensemble of HDX protected oligomers populated during $A\beta$ 40 and $A\beta$ 42 fibril formation correlates with neuronal cell death. Population percentage of each detected ensemble as a function of Δt_{agg} for (A) $A\beta$ 40 pulse-labeled samples where $[M/O]_{NP, A\beta 40}$, $O_P, A\beta 40$, and $F_{A\beta 40}$ are depicted in purple, orange, and green lines, respectively, and for (B) $A\beta$ 42 pulse-labeled samples where $[M/O]_{LP, A\beta 42}$, $O_P, A\beta 42$, and $F_{A\beta 42}$ are depicted in blue, red, and ocre lines, respectively. The corresponding ThT binding measurements for $A\beta$ 40 and $A\beta$ 42 are overlaid in panels A and B, respectively in gray. The maximum intensity of the ThT signal detected during $A\beta$ 40 and $A\beta$ 42 aggregation was adjusted to the maximum relative population of $F_{A\beta 40}$ and $F_{A\beta 42}$, respectively. The data are the mean \pm SD of three experiments. Percentage of primary neuronal survival assessed by means of the MTT assay for (C) $A\beta$ 40 and (D) $A\beta$ 42 aliquots withdrawn at different Δt_{agg} . The final concentration of $A\beta$ 40 and $A\beta$ 42 samples in the media was 5 μ M. The data are the mean \pm SD of at least two independent experiments carried out in quadruplicate.

(Figure 3D). The peak had a width at half height of 2.6 ± 0.1 , somewhat larger than that expected when representing a single species (Figure 3F). The above analysis indicated that this peak corresponded to an ensemble of species that exhibited a moderate degree of protection. Because of that, we denoted it as $[M/O]_{LP, A\beta 42}$ to represent low protected monomers and/or oligomers of $A\beta$ 42. Therefore, compared to $[M/O]_{UP, A\beta 40}$, also detected at the beginning of the lag phase, $[M/O]_{LP, A\beta 42}$ exists as an ensemble of species with some persistent structure, most likely due to intramolecular hydrogen bonding. Differences in structure and/or dynamic properties of the aggregates formed at the beginning of the lag phase by the two variants may offer an explanation for the more aggregation-prone nature of $A\beta$ 42 compared to $A\beta$ 40.

At the end of the ThT lag phase, namely, between 9 and 13 days for $A\beta$ 40 (Figure 3A) and 6 and 8 days for $A\beta$ 42 (Figure 3B), the peaks representing $[M/O]_{UP, A\beta 40}$ and $[M/O]_{LP, A\beta 42}$ in $A\beta$ 40 and $A\beta$ 42 aggregation, respectively, gradually decreased in intensity, while a second lower mass peak already present at the beginning of the lag phase became dominant (Figures 3A,B and 4A,B). This peak showed similar levels of protection against exchange for both $A\beta$ 40 and $A\beta$ 42; 26.1 ± 1.0 of the 39 available amide protons had exchanged to deuterons in $A\beta$ 40 (Figure 3C) and 24.0 ± 1.8 of 41 in $A\beta$ 42 (Figure 3D). The peak width at half height for the $A\beta$ 40 peak was 3.5 ± 0.3 (Figure 3E), while that for $A\beta$ 42 was 2.9 ± 0.1 (Figure 3F). Again, both peak widths were wider than that expected to represent single species. At these time points, a variety of oligomeric assemblies such as annular oligomers and short

protofibrils were visible in the TEM images of both species (Figure 1B and D). Moreover, the number of exposed amides detected for these two ensembles is consistent with previous HDX studies on isolated $A\beta$ oligomers. For example, Wetzel and co-workers found that 60% of the backbone amides, that is, 23 sites, were exposed in $A\beta$ 40 protofibrils.¹⁸ Moreover, Konermann and co-workers established that 24.2 sites were exposed in $A\beta$ -derived diffusible ligands,¹⁹ ADDLs, a stable synthetic $A\beta$ 42 oligomer preparation extensively used in the literature.⁷ We therefore denoted the most abundant peaks observed at the end of the lag phase of $A\beta$ 40 and $A\beta$ 42 aggregation as $O_P, A\beta 40$ and $O_P, A\beta 42$, respectively, representing in each case an ensemble of protected oligomers.

During the growth phase, the peaks corresponding to $O_P, A\beta 40$ and $O_P, A\beta 42$ decreased in intensity, and a third peak at lower mass started to appear, becoming the most abundant species during the plateau phase, from 17 to 24 days for $A\beta$ 40 (Figures 3A and 4A) and from 9 to 11 days for $A\beta$ 42 (Figures 3B and 4B). Since the appearance of this third peak correlated with the development of very significant ThT fluorescence intensity (Figure 4A and B) and the appearance of well-defined fibrils in TEM microographies (Figure 1), we attributed these peaks to fibrils and denoted them as $F_{A\beta 40}$ and $F_{A\beta 42}$, where F stands for fibril. $F_{A\beta 40}$ and $F_{A\beta 42}$ species were the most protected during both $A\beta$ 40 and $A\beta$ 42 aggregation; only 14.5 ± 0.6 amides exchanged with solvent deuterons in $F_{A\beta 40}$ (Figure 3C) and 15.2 ± 0.7 in $F_{A\beta 42}$ (Figure 3D), consistent with previous HDX reports on $A\beta$ fibrils.^{28,29} The peak width was 1.8 ± 0.1 for $F_{A\beta 40}$ (Figure 3E) and 1.9 ± 0.1 for $F_{A\beta 42}$ (Figure 3F). These values are the most similar to those expected to represent single species, thus indicating that $F_{A\beta 40}$ and $F_{A\beta 42}$ represent the most structural homogeneous species formed during aggregation. In summary, the three ensembles detected for each variant show different degrees of protection against HDX, indicating that they represent distinct conformational states and demonstrating that structural transitions occur during $A\beta$ 40 and $A\beta$ 42 aggregation.

Highest Neurotoxicity Is Observed When Ensembles of Protected Oligomers Are Most Abundant. The detection of distinct structural ensembles during $A\beta$ 40 and $A\beta$ 42 fibril assembly allowed us to carry out parallel experiments to determine the relative contribution of each of these ensembles to neural cytotoxicity. To establish the effect of the various samples obtained at different Δt_{agg} in the same primary neuronal culture, we first determined the effect of sample freezing and thawing on the structure of the aggregates. We found that aggregates formed during fibril formation retained their structure after a freeze/thaw cycle as measured by ThT and PL-HDX-ESI-MS (Supplementary Figure S4). We next treated primary hippocampal neuronal cultures with thawed aliquots of the same samples that had been studied in the PL-HDX-ESI-MS experiment and measured the level of neuronal survival by the MTT assay. Exposure of the cultures to 5 μ M $A\beta$ 40 samples corresponding to the beginning of the lag phase, when $[M/O]_{UP, A\beta 40}$ was most abundant, had only a marginal effect on neurotoxicity (at Δt_{agg} of 0 days, $92.6 \pm 0.6\%$) (Figure 4C). However, 5 μ M $A\beta$ 40 samples corresponding to the end of the lag phase, in which $O_P, A\beta 40$ was the most abundant species, showed a considerable decrease in neuronal viability (at Δt_{agg} of 13 days, $65.4 \pm 10.6\%$) as compared to vehicle-treated neurons (100% viability, by definition). Finally, 5 μ M $A\beta$ 40 samples corresponding to the plateau phase showed a minor reduction in viability (at Δt_{agg} of 21 days, 75.0

\pm 8.4%). A similar, although more pronounced, trend was observed when primary cultures were treated with 5 μ M $A\beta$ 42 samples obtained at various time points of aggregation (Figure 4D). Although samples from the beginning of the lag phase and from the plateau phase showed reduced viability (to 79.9 \pm 12.2% and 76.3 \pm 7.9% at Δt_{agg} of 0 and 10 days, respectively), those from the end of the lag phase, in which $O_{P_A\beta42}$ was the most abundant species, showed the largest reduction in viability (to 36.7 \pm 8.2% at Δt_{agg} of 7 days) as compared to vehicle-treated neurons (100% viability, by definition). These results indicate that the presence of an ensemble of protected oligomers, $O_{P_A\beta40}$ and $O_{P_A\beta42}$, is critical for the development of neurotoxicity.

In addition, at time points when the relative abundance of $O_{P_A\beta40}$ and $O_{P_A\beta42}$ is very similar (at Δt_{agg} of 13 days, 72.5 \pm 9.2% and at Δt_{agg} of 7 days, 71.6 \pm 4.8% for $O_{P_A\beta40}$ and $O_{P_A\beta42}$, respectively) the average reduction in cell viability is larger for $O_{P_A\beta42}$ (at Δt_{agg} of 7 days, 36.7 \pm 8.2%) than for $O_{P_A\beta40}$ (at Δt_{agg} of 13 days, 65.4 \pm 10.6%), suggesting that there are specific features within the structure of $O_{P_A\beta42}$ that render them more toxic than $O_{P_A\beta40}$. Compared to $A\beta$ 40, $A\beta$ 42 has two additional hydrophobic residues. It is interesting to speculate that differences in toxicity between $O_{P_A\beta40}$ and $O_{P_A\beta42}$ may arise from the higher fraction of hydrophobic side chains in $O_{P_A\beta42}$ exposed to the solvent.³⁰

Conclusion. Here we have paralleled PL-HDX-ESI-MS experiments with neurotoxicity assays to establish that the development of persistent structure within $A\beta$ oligomers is an important determinant of the neurotoxicity associated with $A\beta$ aggregation. Detection of three distinct structural ensembles and their evolution as a function of time is in agreement with the nucleated conformational conversion (NCC) mechanism of amyloid formation.³¹ NCC proposes that monomers and/or poorly structured oligomers (in our work represented by $[M/O]_{UP_A\beta40}$ and $[M/O]_{LP_A\beta42}$) progress to more structured oligomers ($O_{P_A\beta40}$ and $O_{P_A\beta42}$ in this study) that are not yet locked into a rigid structure capable of evolving into rigid fibril forms ($F_{A\beta40}$ and $F_{A\beta42}$ in this study). Our results are also consistent with a recent study using PL-HDX-ESI-MS to monitor the protection of soluble $A\beta$ 42 aggregates as a function of time.²³ The authors report on two structural reorganizations within the oligomers, the first one being very fast and the second slow. Although the labeling conditions are different, it is likely that the two increases in protection that they observe correspond, respectively, to $[M/O]_{LP_A\beta42}$ and $O_{P_A\beta42}$ in our study. Finally, our results also agree with the findings of a recent study addressing the aggregation of α -synuclein by single molecule fluorescence.³² The authors identify structural rearrangements during α -synuclein aggregation from initially formed oligomers to stable, more compact proteinase-K-resistant oligomers that ultimately lead to fibril formation. In agreement with our results, the more compact oligomers are those that caused the most cell damage.

On the basis of our results, $O_{P_A\beta40}$ and $O_{P_A\beta42}$ could be taken up by cells and generate toxicity directly. However, several reports in the literature suggest that neurotoxicity is not mediated by discrete oligomers but rather by their ability to undergo fibril formation, which depends on the presence of other species present in solution such as monomers.^{13,14} Our results could also be in agreement with this view as in all Δt_{agg} where $O_{P_A\beta40}$ and $O_{P_A\beta42}$ are most abundant; there is coexistence of different species. However, it is remarkable that the populations of HDX protected oligomers, $O_{P_A\beta40}$ and

$O_{P_A\beta42}$, during the period of time when maximum neurotoxicity is observed, suggest so few other species present, such as monomers or unprotected or low protected oligomers and fibrils. Therefore, if the process of aggregation mediates neurotoxicity, our results would suggest that rather than simply originating due to fibril growth by monomer addition, it mainly arises from maturation of the HDX protected oligomers.

Finally, the combination of PL-HDX-ESI-MS experiments with neurotoxicity could be applied to the study of other amyloid diseases and related disorders while offering the exciting prospect of determining the effect of other biological and/or pharmaceutical molecules of relevance on $A\beta$ aggregation and neurotoxicity.

METHODS

Reagents. All reagents were purchased from Sigma-Aldrich unless otherwise specified.

Preparation of $A\beta$ Samples for Aggregation Experiments. $A\beta$ 40 and $A\beta$ 42 variants were synthesized and purified by Dr. James I. Elliott. To obtain monomeric $A\beta$, we used size-exclusion chromatography (SEC). $A\beta$ was dissolved in 6.8 M Gdn-SCN, sonicated for 5 min, diluted to 4 M Gdn-SCN at a 5 mg/mL $A\beta$ concentration, centrifuged at 10,000g for 5 min, and passed through a 0.45- μ m Millex filter. The resulting solution was injected into a HiLoad Superdex 75 HR 16/60 column (GE Healthcare) previously equilibrated with 50 mM NH₄OAc, 1 mM Tris-HCl, and 0.01% NaN₃, pH 7.4, and eluted at a flow rate of 1 mL/min. The system was kept at 4 °C. The peak attributed to monomeric $A\beta$ was collected, and its peptide concentration was determined by HPLC (C4 Symmetry column, Waters in a Waters 2695 HPLC system). HPLC quantification was carried out using a calibration curve generated from $A\beta$ 40 and $A\beta$ 42 solutions previously quantified by amino acid analysis. The $A\beta$ solutions were diluted to 30 μ M and left to aggregate at RT. To carry out ThT binding assay, TEM, X-ray fiber diffraction (Supporting Information Methods), PL-HDX and neurotoxicity experiments, aliquots of the solutions were taken at Δt_{agg} ranging from 0 to 24 days for $A\beta$ 40 and from 0 to 11 days for $A\beta$ 42.

PL-HDX Experiments. Triplicate aliquots of 50 μ L were withdrawn from the aggregating $A\beta$ solutions at a range of Δt_{agg} . The buffer was exchanged to 90% D₂O (Euriso-top) by means of a 1:10 dilution with D₂O. Afterward, the sample was left to exchange for a fixed labeling time (Δt_{label}). Under the aggregation conditions used, a Δt_{label} of 10 s was found to be the minimum controllable time required to exchange all protons to deuterons in a monomeric $A\beta$ 40 sample. After Δt_{label} , samples were freeze-dried to quench exchange.

HDX Analyzed by ESI-MS. To analyze the deuterium content of the samples, lyophilized samples were transferred into a solution of 95% dimethyl sulfoxide-*d*₆ (DMSO-*d*₆, Euriso-top)/5% D₂O at pH* 4.6 (adjusted with dichloroacetic acid-*d*₂), which solubilizes the various aggregates into monomers and preserves the deuterium content of the peptide molecules.²⁷ The samples were dissolved at a 50 μ M concentration in the DMSO-based buffer and immediately injected into a C8 desalting column (Micro Trap 1 mm i.d. \times 8 mm, Michrom Bioresources Inc.). To remove involatile salts and buffers from the sample solution, the C8 column was washed with aqueous acidic solution (H₂O, 0.1% formic acid) for 1 min at a flow of 50 μ L/min. To elute the peptide from the C8 desalting column, a mixture of 80:20 acetonitrile/H₂O was used. The sample was then directly infused at 50 μ L/min into a Waters LCT mass spectrometer (Premier XE, Micromass MS) with a modified ESI probe. Data were collected in positive ion mode, with an applied capillary voltage of 4 kV, a cone voltage of 100 V, a capillary temperature of 20 °C, a gas desolvation flow rate of 300 mL/min, and a cone gas value of 50 mL/min. The same dead time (3 min) was used for sample preparation and parameter adjustment for all measurements. The spectra were analyzed using MassLynx V4.1 (Waters). All mass spectra presented were averages of 25 scans (1 s per scan). $A\beta$ peaks (including +3, +4, and +5 charge states) were observed, and the most abundant +4 charge state

was selected for analysis. To establish the number of species detected during the aggregation of A β 40 and A β 42, triplicate mass spectra for all of the Δt_{agg} studied were globally analyzed and fitted to Gaussian distributions (Supporting Information Methods).

Primary Neuronal Cultures. Hippocampal neurons were obtained from E16 OF1 mouse embryos (Charles River Laboratories). Briefly, brains were dissected in PBS containing 3% glucose, and hippocampi were dissected out. After trypsin (Gibco) and DNase (Roche Diagnostics) treatments, tissue pieces were dissociated by gentle sweeping. Cells were then counted and seeded onto poly-D-lysine-coated dishes in Neurobasal medium containing B27 supplement (Gibco). All experiments involving animals were performed in accordance with the European Community Council directive for the care and use of laboratory animals and were approved by the local ethical committee.

Neuronal Viability Measurements. Primary hippocampal neurons were seeded at 30,000 cells/well in 96-well plates (Costar), maintained for 72–96 h, and then treated with frozen and thawed A β samples obtained at different Δt_{agg} (at final concentrations of 5 μ M) or the corresponding volumes of vehicle (50 mM NH₄OAc, 1 mM Tris, 0.01% NaN₃ at pH 7.4) as a control. After 24 h at 37 °C, neuronal viability was determined using the (3-(4,5-dimethylthiazol-2-yl)-2,5-diphenyltetrazolium bromide (MTT) assay from Roche (Cell Proliferation Kit I). Neuronal viability was expressed as percent of MTT absorbance in treated cells as compared to cognate vehicle-treated cells, which was taken as 100%. The assay was quantified at 595 nm, using the 690 nm absorbance as reference, on an absorbance plate reader.

Summary of Statistical Analysis. GraphPad Prism was used for all statistical analyses. The data are presented as mean \pm SD. The images shown are representative of those obtained in at least three independent experiments.

ASSOCIATED CONTENT

Supporting Information

Supporting methods and figures are available free of charge via the Internet at <http://pubs.acs.org>

AUTHOR INFORMATION

Corresponding Author

*E-mail: natalia.carulla@irbbarcelona.org.

Notes

The authors declare no competing financial interest.

ACKNOWLEDGMENTS

B.S. acknowledges the Spanish Government FPU program for a predoctoral fellowship. We thank Prof. C. M. Dobson, Prof. E. Giralt, and Prof. C. Woodward for helpful discussions and critical reading of the manuscript, the Mass Spectrometry Core Facility at IRB Barcelona for technical support, and T. Yates for editorial help. This work was supported by Program Grants from the MINECO-FEDER (SAF2012-35226) to N.C. and from the Alzheimer's Association (NIRP-12-256641) to N.C.

REFERENCES

- (1) Masters, C. L., and Selkoe, D. J. (2012) Biochemistry of amyloid beta-protein and amyloid deposits in Alzheimer disease. *Cold Spring Harbor Perspect. Med.* 2, a006262.
- (2) Serpell, L. C. (2000) Alzheimer's amyloid fibrils: structure and assembly. *Biochim. Biophys. Acta* 1502, 16–30.
- (3) Dickson, D. W., Crystal, H. A., Bevona, C., Honer, W., Vincent, I., and Davies, P. (1995) Correlations of synaptic and pathological markers with cognition of the elderly. *Neurobiol. Aging* 16, 285–298.
- (4) McLean, C. A., Cherny, R. A., Fraser, F. W., Fuller, S. J., Smith, M. J., Beyreuther, K., Bush, A. I., and Masters, C. L. (1999) Soluble pool of Abeta amyloid as a determinant of severity of neurodegeneration in Alzheimer's disease. *Ann. Neurol.* 46, 860–866.
- (5) Haass, C., and Selkoe, D. J. (2007) Soluble protein oligomers in neurodegeneration: lessons from the Alzheimer's amyloid beta-peptide. *Nat. Rev. Mol. Cell Biol.* 8, 101–112.
- (6) Benilova, I., Karan, E., and De Strooper, B. (2012) The toxic Abeta oligomer and Alzheimer's disease: an emperor in need of clothes. *Nat. Neurosci.* 15, 349–357.
- (7) Lambert, M. P., Barlow, A. K., Chromy, B. A., Edwards, C., Freed, R., Liosatos, M., Morgan, T. E., Rozovsky, I., Trommer, B., Viola, K. L., Wals, P., Zhang, C., Finch, C. E., Krafft, G. A., and Klein, W. L. (1998) Diffusible, nonfibrillar ligands derived from Abeta1–42 are potent central nervous system neurotoxins. *Proc. Natl. Acad. Sci. U.S.A.* 95, 6448–6453.
- (8) Chimon, S., Shaibat, M. A., Jones, C. R., Calero, D. C., Aizezi, B., and Ishii, Y. (2007) Evidence of fibril-like beta-sheet structures in a neurotoxic amyloid intermediate of Alzheimer's beta-amyloid. *Nat. Struct. Mol. Biol.* 14, 1157–1164.
- (9) Yu, L., Edalji, R., Harlan, J. E., Holzman, T. F., Lopez, A. P., Labkovsky, B., Hillen, H., Barghorn, S., Ebert, U., Richardson, P. L., Miesbauer, L., Solomon, L., Bartley, D., Walter, K., Johnson, R. W., Hajduk, P. J., and Olejniczak, E. T. (2009) Structural characterization of a soluble amyloid beta-peptide oligomer. *Biochemistry* 48, 1870–1877.
- (10) Ahmed, M., Davis, J., Aucoin, D., Sato, T., Ahuja, S., Aimoto, S., Elliott, J. I., Van Nostrand, W. E., and Smith, S. O. (2010) Structural conversion of neurotoxic amyloid-beta(1–42) oligomers to fibrils. *Nat. Struct. Mol. Biol.* 17, 561–567.
- (11) Haupt, C., Leppert, J., Ronicke, R., Meinhardt, J., Yadav, J. K., Ramachandran, R., Ohlenschlager, O., Reymann, K. G., Gorlach, M., and Fandrich, M. (2012) Structural basis of beta-amyloid-dependent synaptic dysfunctions. *Angew. Chem., Int. Ed.* 51, 1576–1579.
- (12) Cohen, S. I., Linse, S., Luheshi, L. M., Hellstrand, E., White, D. A., Rajah, L., Otzen, D. E., Vendruscolo, M., Dobson, C. M., and Knowles, T. P. J. (2013) Proliferation of amyloid-beta42 aggregates occurs through a secondary nucleation mechanism. *Proc. Natl. Acad. Sci. U.S.A.* 110, 9758–9763.
- (13) Wogulis, M., Wright, S., Cunningham, D., Chilcote, T., Powell, K., and Rydel, R. E. (2005) Nucleation-dependent polymerization is an essential component of amyloid-mediated neuronal cell death. *J. Neurosci.* 25, 1071–1080.
- (14) Jan, A., Adolfsson, O., Allaman, I., Buccarello, A. L., Magistretti, P. J., Pfeifer, A., Muhs, A., and Lashuel, H. A. (2011) Abeta42 neurotoxicity is mediated by ongoing nucleated polymerization process rather than by discrete Abeta42 species. *J. Biol. Chem.* 286, 8585–8596.
- (15) Bernstein, S. L., Dupuis, N. F., Lazo, N. D., Wyttenbach, T., Condon, M. M., Bitan, G., Teplow, D. B., Shea, J. E., Ruotolo, B. T., Robinson, C. V., and Bowers, M. T. (2009) Amyloid-beta protein oligomerization and the importance of tetramers and dodecamers in the aetiology of Alzheimer's disease. *Nat. Chem.* 1, 326–331.
- (16) Narayan, P., Orte, A., Clarke, R. W., Bolognesi, B., Hook, S., Ganitzer, K. A., Meehan, S., Wilson, M. R., Dobson, C. M., and Klenerman, D. (2012) The extracellular chaperone clusterin sequesters oligomeric forms of the amyloid-beta(1–40) peptide. *Nat. Struct. Mol. Biol.* 19, 79–83.
- (17) Konermann, L., Vahidi, S., and Sowole, M. A. (2014) Mass spectrometry methods for studying structure and dynamics of biological macromolecules. *Anal. Chem.* 86, 213–232.
- (18) Kheterpal, I., Lashuel, H. A., Hartley, D. M., Walz, T., Lansbury, P. T., Jr., and Wetzel, R. (2003) Abeta protofibrils possess a stable core structure resistant to hydrogen exchange. *Biochemistry* 42, 14092–14098.
- (19) Pan, J., Han, J., Borchers, C. H., and Konermann, L. (2011) Conformer-specific hydrogen exchange analysis of Abeta(1–42) oligomers by top-down electron capture dissociation mass spectrometry. *Anal. Chem.* 83, 5386–5393.
- (20) Pan, J., Han, J., Borchers, C. H., and Konermann, L. (2012) Structure and dynamics of small soluble Abeta(1–40) oligomers

studied by top-down hydrogen exchange mass spectrometry.

Biochemistry 51, 3694–3703.

(21) Mysling, S., Betzer, C., Jensen, P. H., and Jorgensen, T. J. D.

(2013) Characterizing the dynamics of alpha-synuclein oligomers using hydrogen/deuterium exchange monitored by mass spectrometry.

Biochemistry 52, 9097–9103.

(22) Paslawski, W., Mysling, S., Thomsen, K., Jorgensen, T. J. D., and

Otzen, D. E. (2014) Co-existence of two different alpha-synuclein

oligomers with different core structures determined by hydrogen/

deuterium exchange mass spectrometry. *Angew. Chem., Int. Ed.* 53,

7560–7563.

(23) Zhang, Y., Rempel, D. L., Zhang, J., Sharma, A. K., Mirica, L. M.,

and Gross, M. L. (2013) Pulsed hydrogen-deuterium exchange mass

spectrometry probes conformational changes in amyloid beta (Abeta)

peptide aggregation. *Proc. Natl. Acad. Sci. U.S.A.* 110, 14604–14609.

(24) Carulla, N., Zhou, M., Arimon, M., Gairi, M., Giralt, E.,

Robinson, C. V., and Dobson, C. M. (2009) Experimental character-

ization of disordered and ordered aggregates populated during the

process of amyloid fibril formation. *Proc. Natl. Acad. Sci. U.S.A.* 106,

7828–7833.

(25) Jan, A., Hartley, D. M., and Lashuel, H. A. (2010) Preparation

and characterization of toxic Abeta aggregates for structural and

functional studies in Alzheimer's disease research. *Nat. Protoc.* 5,

1186–1209.

(26) Reinke, A. A., and Gestwicki, J. E. (2011) Insight into amyloid

structure using chemical probes. *Chem. Biol. Drug Des.* 77, 399–411.

(27) Sanchez, L., Madurga, S., Pukala, T., Vilaseca, M., Lopez-Iglesias,

C., Robinson, C. V., Giralt, E., and Carulla, N. (2011) Abeta40 and

Abeta42 amyloid fibrils exhibit distinct molecular recycling properties.

J. Am. Chem. Soc. 133, 6505–6508.

(28) Kheterpal, I., Zhou, S., Cook, K. D., and Wetzel, R. (2000)

Abeta amyloid fibrils possess a core structure highly resistant to

hydrogen exchange. *Proc. Natl. Acad. Sci. U.S.A.* 97, 13597–13601.

(29) Luhrs, T., Ritter, C., Adrian, M., Riek-Loher, D., Bohrmann, B.,

Dobeli, H., Schubert, D., and Riek, R. (2005) 3D structure of

Alzheimer's amyloid-beta(1–42) fibrils. *Proc. Natl. Acad. Sci. U.S.A.*

102, 17342–17347.

(30) Campioni, S., Mannini, B., Zampagni, M., Pensalfini, A., Parrini,

C., Evangelisti, E., Relini, A., Stefani, M., Dobson, C. M., Cecchi, C.,

and Chiti, F. (2010) A causative link between the structure of aberrant

protein oligomers and their toxicity. *Nat. Chem. Biol.* 6, 140–147.

(31) Serio, T. R., Cashikar, A. G., Kowal, A. S., Sawicki, G. J.,

Moslehi, J. J., Serpell, L., Arnsdorf, M. F., and Lindquist, S. L. (2000)

Nucleated conformational conversion and the replication of conforma-

tional information by a prion determinant. *Science* 289, 1317–1321.

(32) Cremades, N., Cohen, S. I., Deas, E., Abramov, A. Y., Chen, A.

Y., Orte, A., Sandal, M., Clarke, R. W., Dunne, P., Aprile, F. A.,

Bertoncini, C. W., Wood, N. W., Knowles, T. P. J., Dobson, C. M., and

Klenerman, D. (2012) Direct observation of the interconversion of

normal and toxic forms of alpha-synuclein. *Cell* 149, 1048–1059.